Available online at www.sciencedirect.com
SCIENCE DIRECT®
Journal of Nuclear Materials 326 (2004) 19–29
journal of nuclear materials
www.elsevier.com/locate/jnucmat

Irradiation damage in 304 and 316 stainless steels: experimental investigation and modeling. Part I: Evolution of the microstructure

C. Pokor [a,b], Y. Brechet [c], P. Dubuisson [a], J.-P. Massoud [d,*], A. Barbu [e]

[a] CEA/DEN/SRMA, CEA Saclay, 91191 Gif sur Yvette cedex, France
[b] EDF/GDL/SECH, BP23-37420 Avoine cedex, France
[c] LTPCM, BP75, Domaine Universitaire de Grenoble, 38402 Saint Martin d'Heres cedex, France
[d] EDF R&D, MMC, Site des Renardières, 77818 Moret sur Loing cedex, France
[e] CEA/DEN/SRMP, CEA Saclay, 91191 Gif sur Yvette cedex, France

Received 6 August 2003; accepted 15 November 2003

Abstract

Irradiation damage in three austenitic stainless steels, SA 304L, CW 316 and CW Ti-modified 316, is investigated both experimentally and theoretically. The density and size of Frank loops after irradiation at 320 and 375 °C in experimental EBR II, BOR-60 and OSIRIS reactors for doses up to 40 dpa are characterized by TEM. The evolution of the initial dislocation network under irradiation is evaluated. A cluster dynamics model is proposed to account quantitatively for the experimental findings.
© 2003 Elsevier B.V. All rights reserved.

PACS: 61.80; 61.72.F; 21.60.G

1. Introduction

The internal structures of pressurized water reactors (PWR) located close to the reactor core are used to support the fuel assemblies, to maintain the alignment between assemblies and the control bars and to canalize the primary water. In general these internal structures consist of baffle plates in Solution Annealed 304 stainless steel and baffle bolts in Cold Worked 316 stainless steel. These components undergo a large neutron flux at temperatures between 280 and 380 °C. As a result, the material exhibits a substantial increase in yield stress and reduction in ductility which may be damaging to the proper operation of the reactor. For instance the observed cracks in bolts, usually attributed to irradiation assisted stress corrosion cracking (IASCC), can be seen as a consequence of the evolution of plasticity in these materials loaded in a corrosive medium, together with possible evolutions of grain boundary chemistry (Radiation Induced Segregation) which is well documented [1]. This irradiation induced embrittlement becomes more pronounced with increasing irradiation dose, thus being an important and limiting factor in ageing reactors. Of special interest is the question of the possible saturation of microstructural evolution and related hardening for long term irradiation. In the present contribution, we will focus our attention on the evolution of the structural defects induced by irradiation and on their consequences on the yield stress, which we acknowledge as

* Corresponding author. Tel.: +33-1 60 73 71 05; fax: +33-1 60 73 68 89.
E-mail address: jean-paul.massoud@edf.fr (J.-P. Massoud).

0022-3115/$ - see front matter © 2003 Elsevier B.V. All rights reserved.
doi:10.1016/j.jnucmat.2003.11.007

being only one of the contribution to embrittlement phenomenon. This evolution in mechanical properties depends both on the initial metallurgical state of the alloy and on the irradiation conditions (temperature, flux, dose, and neutron energy spectrum). It is associated with a microstructural evolution resulting from the production and the collective dynamics of irradiation point defects, leading to the formation of dislocation loops and cavities, and to the evolution of the initial dislocation network. In order to rationalize the effects of irradiation conditions, and to predict the long term behavior from the observations for smaller doses, it is necessary to develop models able to describe, on one side the microstructural evolutions, and on the other side the resulting hardening effects. The parameters entering these models have to be identified from a quantitative description of the microstructure and yield stresses, and the prediction of the models have to be validated by comparison with experiments for larger dose. The aim of the two companion papers is to provide with quantitative characterization of irradiation defects by TEM (paper I) and of mechanical properties (yield stress) after irradiation by tensile test at constant strain rates (paper II). The modeling of microstructure evolution will be done using a cluster dynamics approach (paper I) whereas the evolution of yield stress for a given microstructure will be modeled using classical dislocation theory (paper II).

The two papers are structured as follows: in paper I, we present the materials investigated, the irradiation conditions and the characterization methods (Section 2). The experimental results concerning the microstructures for the different alloys and irradiation conditions will be presented in Section 3. The principles of the cluster dynamic model, the identification of the parameters and the predictions are developed and compared with experimental results in Section 4. In paper II, Section 1 recalls the proposed mechanism for the evolution of yield stress, and summarizes briefly and qualitatively the findings of paper I, whereas Section 2 presents the experimental conditions for tensile testing and the measured yield stresses for the different alloys and irradiation conditions. In Section 3 we propose a model for the yield stress evolution coupling the hardening by dislocation loops and the question of their stability, and we compare the predictions of this model with the experimental results.

2. Materials, irradiation conditions and characterization methods

2.1. Materials

The alloys for the microstructural characterization after neutron irradiation are 300 series stainless steels commonly used in PWR internals: Solution Annealed 304L (used for baffle plates) and Cold Worked 316 (used for baffle bolts). In addition, an exploratory material such as modified 316 containing a small amount of Ti, has been investigated. The chemical compositions of the three alloys are provided in Table 1. The choice of the alloys was motivated by their relevance in actual reactors. The influence of chemical composition and initial state of deformation is of relevance for guiding possible material evolution.

The standard 304L steel is solution annealed, the microstructure consisting of recrystallized grains ($\sim$ 40 μm) containing few dislocations and a small amount of ferrite (<1%).

The standard 316 steel is 15% cold worked, it is fully austenitic, and it contains more Ni and Mo and less Cr than the SA 304L steel. The grain size is about 40 μm.

The modified 316 stainless steel contains a slightly higher value of Si (0.83%) and Mn (1.9%) and a small amount of Ti (0.28%). It is 20% cold worked. Ti addition is known in the literature to stabilize the dislocation network via a solid solution hardening effect [2]. The grain size is about 40 μm.

The initial microstructures before irradiation for the three alloys are shown in Fig. 1. As expected from the difference in initial deformation sequences, the 316 steels contain numerous dislocations organized in a cell structure, and deformation twins (Fig. 1(b) and (c)).

2.2. Irradiation conditions

The irradiation conditions in terms of temperatures and doses were selected to be representative of the various situations encountered in operation conditions of PWRs. In order to reach representative doses in a reasonable time, the use of fast breeder reactors with higher fluxes was required.

The irradiations were realized in two types of experimental reactors: fast breeder reactors (EBRII and BOR-60) and a reactor presenting a mixed neutron

Table 1
Chemical composition of the steels (wt%)

Steel	C	S	P	Si	Mn	Ni	Cr	N	Mo	Cu	Co	B	Ti
SA304	0.022	0.0007	0.032	0.36	1.79	9.86	18.61	0.061	–	0.25	0.064	0.0005	–
316	0.054	0.0220	0.027	0.68	1.12	10.60	16.60	0.023	2.25	0.24	0.120	0.0005	<0.01
316Ti	0.058	0.0070	0.021	0.83	1.90	12.80	17.40	0.028	2.36	0.05	0.050	<0.0025	0.28

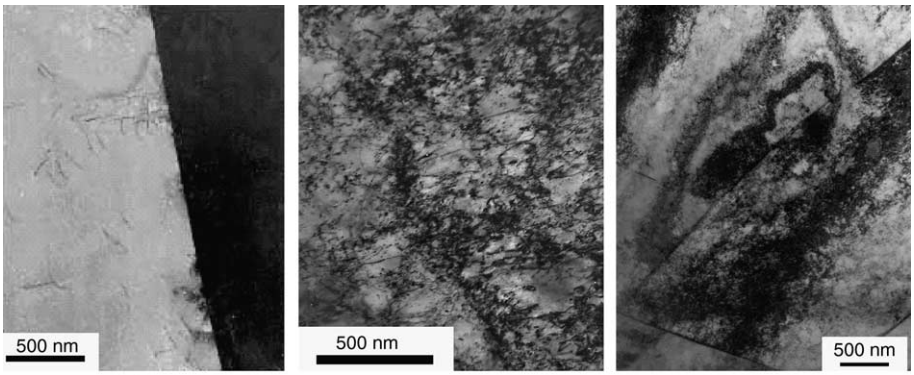

Fig. 1. General aspect in TEM of the steels (a) SA 304, (b) CW 316 and (c) CW 316 Ti.

Table 2
Irradiation conditions

Reactor name	Fast flux (dpa/s)	Temp. (°C)	Doses (dpa)
EBR-II (Idaho Falls, US)	1.4×10^{-6}	~375	8–10
BOR-60 (Dimitrovgrad, Russia)	9.4×10^{-7}	~320	10–20–40
OSIRIS (Saclay, France)	2.9×10^{-7}	~330	0.8–3.4

spectrum (OSIRIS). The characteristics in terms of flux, temperature and doses (dpa-NRT), and the locations of the experimental facilities are presented in Table 2.

2.3. Microstructural characterization techniques

The irradiated microstructure was quantitatively investigated using transmission electron microscopy. The TEM samples have been extracted from the head of tensile test specimens irradiated in experimental reactors. The thin foils are obtained by mechanical thinning down to 100 μm, followed by electrolytic thinning in a solution of 70% of ethanol, 20% of ethylene glycol monobutylic ether and 10% of perchloric acid. The operating temperature and voltage are 10 °C and 20 V. As the materials were radioactive, all the sample preparations had to be performed in Hot Cells and Glove Boxes.

The TEM observations were performed on a EM 430 Philips microscope, with LaB_6 filament and a tension of 300 kV. Bright field, dark field, weak beam dark field and microdiffraction techniques were used in order to identify and quantify the structural defects resulting from irradiation.

The imaging of faulted Frank loops located in all sets of {1 1 1} planes, necessary to measure their sizes, were obtained using the Reciprocal Lattice Rod technique [3], taking advantage of the stacking fault present inside these loops. In order to estimate the number of loops per unit volume, the thickness of the thin foil was evaluated by stereoscopy.

The cavities are identified and quantified on bright field images out of contrast: they appear as tiny spherical objects.

The results of microstructural characterizations were provided in terms of average sizes and densities. In addition, the size histograms for the various defects are provided.

3. Experimental results

The experimental results for the three alloys are presented for each irradiation temperature. We present first the microstructure after irradiation at the intermediate temperature (330 °C) obtained either in the mixed flux reactor OSIRIS at low irradiation doses or in the fast breeder BOR-60 reactor for the higher irradiation doses. We then give the results concerning the irradiation at the highest temperature (375 °C) in the fast breeder reactor EBR-II.

3.1. Irradiation at 330 °C

The three alloys irradiated at 330 °C have a similar microstructure. For doses up to 3.4 dpa, it consists in interstitial Frank loops located in the {1 1 1} planes with a Burgers vector of $b = \langle 111 \rangle$ and of 'black dots'. Fig. 2 shows bright field images for the three alloys irradiated at 0.8 dpa. Most of the initial dislocation structure has disappeared during irradiation. Neither irradiation induced precipitation nor cavity was observed.

There is some controversy in the literature concerning the nature of 'black dots'. At low dose (0.8 dpa), when both Frank loops and 'black dots' can be observed simultaneously, we were able to obtain the size distribution of the two types of defects. The 'black dots' are imaged in bright field, and the Frank loops in dark field.

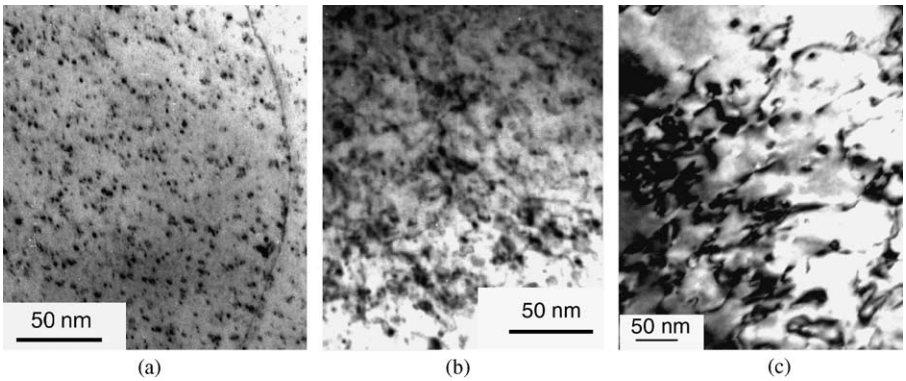

Fig. 2. Bright field images of the alloys irradiated at 330 °C for a dose of 0.8 dpa (a) SA 304, (b) CW 316 and (c) CW 316Ti.

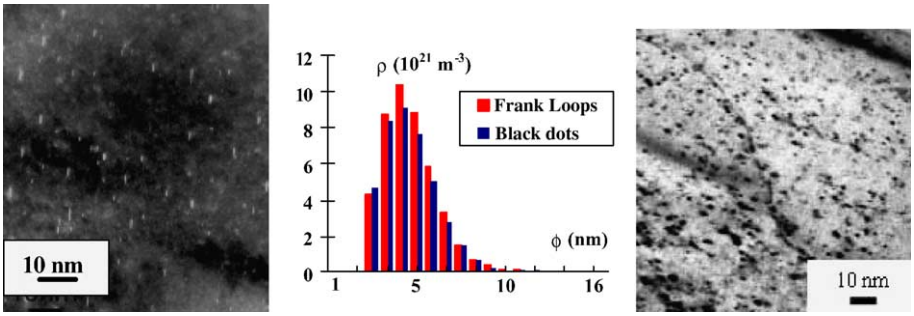

Fig. 3. (a) Imaging of Frank loops, (b) size histogram and (c) black dots in SA 304 irradiated at 330 °C for a dose of 0.8 dpa.

The average size, the density and the size distributions of the two families are identical (Fig. 3). We claim that 'black dots' and small Frank loops are one single defect seen under different contrast conditions.

When the dose increases (up to 40 dpa, obtained by irradiation in BOR-60 reactor), the size and density of Frank loops increase. The quantitative results for the average loop size and the loop density for the three steels and the various doses are shown in Table 3. The microstructure evolution is rapid for doses under 10 dpa, and tends to saturate for larger doses.

From the comparison between the three alloys, it appears that at high and similar doses, the 304L and 316 alloys exhibit similar loop sizes, whereas the loops are larger for the Ti-modified 316 steel. The loop density is higher for the 304L steel, followed by the 316 and Ti-modified 316 steels.

3.2. Irradiation at 375 °C

The 304L samples show a typical microstructure of irradiated austenitic steels, with a gray contrast due to a high density of very small objects homogeneously distributed inside the grains (Fig. 4(a)). No irradiation induced precipitation was observed. An homogeneous distribution of cavities was identified (Fig. 4(b)).

Table 3
Quantitative characterization of Frank loops at 330 °C for the three alloys

Alloy	Dose (dpa)	Frank loop diameter (nm) ±2 nm	Frank loop density (m^{-3})
SA 304	0.8	4.7	45×10^{21}
	2	5.9	74×10^{21}
	3.4	7.4	63×10^{21}
	20	7.3	62×10^{21}
	40	7.0	77×10^{21}
CW 316	0.8	9.3	28×10^{21}
	2	7.7	28.8×10^{21}
	3.4	10	31×10^{21}
	10	7.5	60×10^{21}
	20	7.4	44×10^{21}
	40	7.3	62×10^{21}
CW 316Ti	0.8	Few small loops	
	2	6.9	13×10^{21}
	3.4	5.7	24×10^{21}
	40	9.8	50×10^{21}

The 316 alloy shows a similar contrast (Fig. 4(c)). The initial dislocation network has totally disappeared. The twins initially present are still there. No precipita-

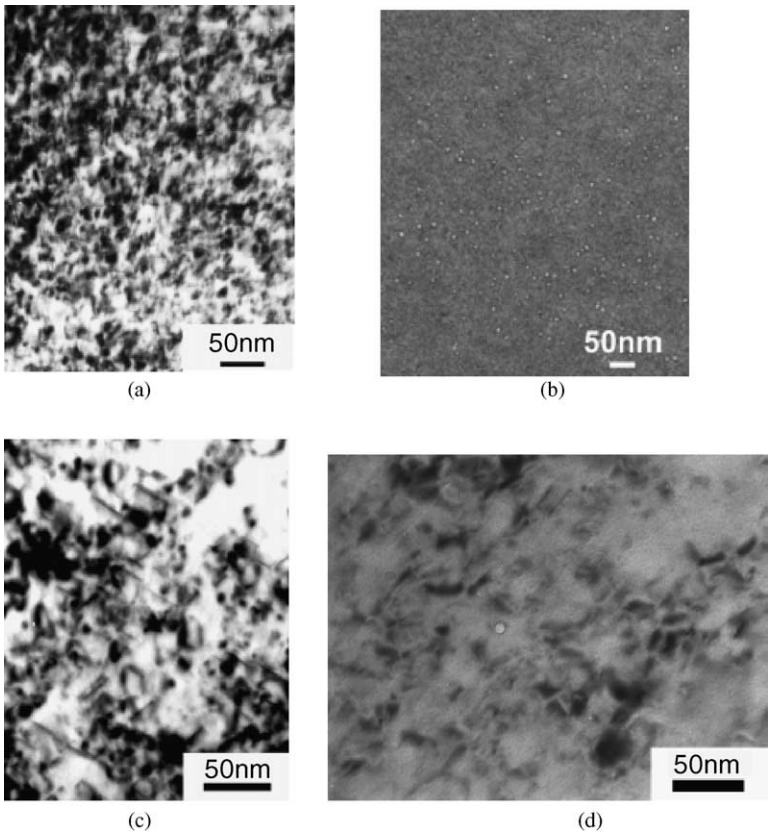

Fig. 4. (a), (b) 304 and (c), (d) 316 alloy irradiated at 375 °C for a dose of 10 dpa – imaging of Frank loops and cavities.

Table 4
Quantitative characterization of Frank loops and cavities at 375 °C, for the two alloys

Alloy	Dose (dpa)	Frank loop diameter (nm)	Frank loop density (m^{-3})	Cavity diameter (nm)	Cavity density (m^{-3})
SA304	8	11.5	30×10^{21}	Not measurable	Not measurable
	10	12.4	33×10^{21}	5.4	4.7×10^{21}
CW316	8	12.1	32×10^{21}	Not measurable	Not measurable
	10	12.2	32×10^{21}	4.6	Few

tion is evidenced. Very few cavities are observed (Fig. 4(d)).

Quantitative results for both cavities and Frank loops at the various doses are shown in Table 4.

The comparison between the various alloys leads to conclusions similar to the ones reached for irradiations at 330 °C. The comparison between temperatures for a given alloy at a given dose shows that a higher irradiation temperature leads to larger loops with a smaller density. Cavities which were absent at low temperature appear at higher temperatures, especially in solution annealed 304L steel. The initial dislocation network, especially in cold worked 316 steel is more completely recovered at higher temperatures.

4. Modeling

The physical reasons for irradiation damage stems from the collective behavior of the point defects created during irradiation. For a given neutron flux, the number of vacancies and interstitials, and more generally, the number of groups of point defects effectively created after a collision depends on the energy of the incoming neutron, and on the events taking place at the atomistic level in the irradiation cascade. There exists a considerable amount of simulation work, mainly using molecular dynamics for cascade simulations, and kinetic Monte Carlo for rearrangements, dealing with this process of generating the point defects. We are interested

in the scale above the individual cascade event, focusing on the collective behavior of such defects, in excess of their thermodynamic equilibrium values.

These defects, able to diffuse, can either annihilate on external sinks (such as pre-existing dislocations or grain boundaries), or undergo mutual annihilations as vacancy/interstitial pairs, or recombine creating dislocation loops or voids. In the present situation, since we have neglected the possible production of gases which are known to contribute to cavity formation, we will restrict our modeling to the evolution of dislocation loop population in the presence of a supersaturation of diffusing point defects.

The model described was originally developed for ferritic steels at low doses (lower than 0.1 dpa) [7], corresponding to the materials and the irradiation conditions of pressure vessels. We have adapted this model to the case of austenitic steels for large doses, which is relevant to the PWR internal structures. The differences between the ferritic steels and the austenitic steels are represented in the model by differences between the values of the materials parameters such as the formation energies, the binding energies, the lattice parameter and the Burgers vector of the loops. No modification of the model is necessary to take into account the higher exposure (40 dpa compared to 0,1 dpa), it is just a question of calculation time. In addition, as the austenitic materials were cold worked, it is necessary to take into account the evolution of the initial dislocation structure. The basic equations of the model are first recalled in Section 4.1 and the results are compared with experimental observations in Section 4.2.

4.1. Principles of the cluster dynamics model

The principle of the model used here is to describe a population of loops by its size distribution (either discretized as loops containing n point defects, or continuously as loops of radius r). The evolution of this population is obtained via a 'chemical kinetics' in an homogeneous medium, where the probability for a cluster of n point defects to become a cluster of size $n+1$ or $n-1$ depends on its rate of absorption or emission of a vacancy or an interstitial. These kinetics depend on the available population of mobile defects.

The necessary ingredients for such a model are:

- rate of production of defects from the irradiation cascade $G_{\mathrm{v}}(n)$ and $G_{\mathrm{i}}(n)$,
- reaction kinetics between point defects,
- absorption and emission of point defects by and from clusters of point defects (loops),
- annihilation kinetics on fixed sinks such as grain boundaries,
- annihilation kinetics on dislocations and resulting evolution of the dislocation network.

The model will consist in solving a set of coupled equations: two equations for individual vacancies or interstitials, and $2N$ for the population of loops, either of interstitial or vacancy nature, consisting of n defects (n being between 2 and $N+1$). In the following, the subscript i means 'interstitials' and the subscript v means 'vacancies'. For instance $C_{\mathrm{i}}(n)$ is the number of clusters of n interstitials per unit volume. For the sake of simplicity, it is assumed that only the point defects are able to diffuse. The elementary evolution step for a cluster of size n is to evolve toward a cluster of size $n+1$ or $n-1$.

The solution of these coupled equations will be obtained either solving a linear system of discrete equations for loops of size smaller than 100, or solving a Fokker–Planck continuum equation for larger loops.

The generation of defects from the cascades, and its relation with the irradiation conditions, has to be inferred from molecular dynamics simulations. From [4] we have chosen to consider that clusters of size larger than 4 are unlikely to occur:

$$G_{\mathrm{i}}(1) = \eta G_{\mathrm{dpa}}(1 - f_{\mathrm{i}2} - f_{\mathrm{i}3} - f_{\mathrm{i}4}), \tag{1a}$$

$$G_{\mathrm{i}}(2) = \eta G_{\mathrm{dpa}} f_{\mathrm{i}2}, \tag{1b}$$

$$G_{\mathrm{i}}(3) = \eta G_{\mathrm{dpa}} f_{\mathrm{i}3}, \tag{1c}$$

$$G_{\mathrm{i}}(4) = \eta G_{\mathrm{dpa}} f_{\mathrm{i}4}, \tag{1d}$$

$$G_{\mathrm{i}}(n > 4) = 0. \tag{1e}$$

A similar expression is written for $G_{\mathrm{v}}(n)$. G_{dpa} is the neutron flux in the reactor, η is the cascade efficiency and f_{in} is the fraction of clusters of size n and type i surviving the reorganization events following the cascade. These quantities depend in principle on the irradiation temperature and on the energy of the incident neutron. Estimations for these quantities can be obtained from molecular dynamic simulations performed on pure Fe [5]. We have used these quantities as adjustable parameters (in an acceptable range) to describe the difference between the various energy spectra corresponding to the experimental reactors.

The general form of the equation to be solved is:

- For the clusters of size n, the concentrations per unit volume $C_{\mathrm{i}}(n)$ and $C_{\mathrm{v}}(n)$:

$$\frac{\mathrm{d}C_{\mathrm{i}}(n)}{\mathrm{d}t} = G_{\mathrm{i}}(n) + a_{\mathrm{i},n+1}C_{\mathrm{i}}(n+1) - b_{\mathrm{i},n}C_{\mathrm{i}}(n) + c_{\mathrm{i},n-1}C_{\mathrm{i}}(n-1). \tag{2a}$$

Here $a_{\mathrm{i},n+1}$ is the combined rate of emission of an interstitial and absorption of a vacancy by an interstitial loop of size $n+1$, both events leading to an interstitial loop of size n. A loop of size n can evolve toward a loop of size

$n+1$ absorbing an interstitial, or toward a loop of size $n-1$ absorbing a vacancy or emitting an interstitial. Finally, an interstitial loop of size $n-1$ can evolve into a loop of size n by absorbing an interstitial. For the sake of simplicity, the emission of vacancies from an interstitial loop and of interstitials from vacancy loops is not allowed, being energetically too costly for small loops such as the ones obtained with the model [7]. As a consequence the coefficients $a_{i,n}$, $b_{i,n}$ and $c_{i,n}$ are related to the density of free point defects $C_i(1)$ and $C_v(1)$ and the rates of emission and absorption β and α. For instance, $\beta_{k,j}(n)$ is the rate of absorption of a defect of type j by a loop of type k and of size n and $\alpha_{k,j}(n)$ is the rate of emission of a defect of type j by a loop of type k and of size n. Following these notations, the expression for $a_{i,n}$, $b_{i,n}$, and $c_{i,n}$ are:

$$a_{i,n+1} = \beta_{i,v}(n+1)C_v(1) + \alpha_{i,i}(n+1), \tag{2b}$$

$$b_{i,n} = \beta_{i,v}(n)C_v(1) + \beta_{i,i}(n)C_i(1) + \alpha_{i,i}(n), \tag{2c}$$

$$c_{i,n-1} = \beta_{i,i}(n-1)C_i(1). \tag{2d}$$

A similar set of equations can be written for the evolution of the vacancies loops $C_v(n)$.

- For the point defects concentrations per unit volume $C_i(1)$ and $C_v(1)$, one can write:

$$\frac{dC_i(1)}{dt} = G_i(1) - R_{iv}C_i(1)C_v(1) - \frac{C_i(1)}{\tau^a_{d,i}} - \frac{C_i(1)}{\tau^a_{gb,i}} - \frac{C_i(1)}{\tau^a_i(n)} + \frac{1}{\tau^e_i(n)}. \tag{3a}$$

Here $\tau^a_j(n)$ and τ^e_j are the characteristic times for absorbing or emitting a defect of type j by the population of interstitial or vacancy clusters of size up to n. These quantities are related to the α and β via Eqs. (2b)–(2d).

$$\frac{1}{\tau^e_i(n)} = \sum_{n>2} \alpha_{i,i}(n)C_i(n) + 4\alpha_{i,i}(2)C_i(2) + \beta_{i,v}(2)C_vC_i(2), \tag{3b}$$

$$\frac{1}{\tau^a_i(n)} = \sum_{n>0} \beta_{i,i}(n)C_i(n) + \sum_{n>1} \beta_{v,i}(n)C_v(n). \tag{3c}$$

The characteristic annihilation rate R_{iv} of vacancy and interstitial can be written:

$$R_{iv} = 4\pi(D_i + D_v)r_{i,v}, \tag{3d}$$

where D_i and D_v are the diffusion coefficients of interstitials and vacancies respectively, and $r_{i,v}$ is a recombination radius.

The characteristic times for annihilation on grain boundaries $\tau^a_{gb,i}$ and dislocations $\tau^a_{d,i}$ depend on the grain size d and on the dislocation density ρ. Following Brailsford and Bullough [6], these quantities can be expressed as follows:

$$\frac{1}{\tau^a_{d,i}} = \rho D_i Z_i, \tag{3e}$$

$$\frac{1}{\tau^a_{gb,i}} = 6D_i \frac{\sqrt{\rho_D Z_i + \sum_n \beta_{i,i}(n)C_i(n) + \sum_n \beta_{v,i}(n)C_v(n)}}{d}. \tag{3f}$$

A similar set of expressions can be obtained for the equivalent terms for the vacancies.

The physics of the problem is therefore contained in the expressions for α and β

$$\alpha_{i,i}(n) = 2\pi r_i(n)Z_{ic}\frac{D_i}{V_{at}}\exp\left(-\frac{E_{bi}(n)}{kT}\right), \tag{4a}$$

$$\beta_{i,i}(n) = 2\pi r_i(n)Z_{ic}D_i, \tag{4b}$$

$$\beta_{i,v}(n) = 2\pi r_i(n)Z_{ic}D_v, \tag{4c}$$

$$\alpha_{v,v}(n) = 2\pi r_v(n)Z_{vc}D_v\exp\left(-\frac{E_{bv}(n)}{kT}\right), \tag{4d}$$

$$\beta_{v,v}(n) = 2\pi r_v(n)Z_{vc}D_v, \tag{4e}$$

$$\beta_{v,i}(n) = 2\pi r_v(n)Z_{ic}D_i. \tag{4f}$$

In these expressions, $r_j(n)$ is the size of the cluster of type j containing n point defects, V_{at} is the atomic volume, T is the temperature and k is the Boltzmann constant. The important parameters are the bias factors $Z_{ic}(n)$ (resp. $Z_{vc}(n)$) for interstitials (respectively vacancies) of clusters of size n. This bias is independent of the nature of the loop [21] but depends on the size of the loop. Following [7] this bias can be expressed as:

$$Z_{ic} = Z_i + \left(\sqrt{\frac{b}{8\pi a}}Z_{li} - Z_i\right)(1/n^{a_{li}/2}), \tag{5}$$

where Z_i is the bias factor for an infinite straight dislocation for the interstitial point defects, a is the lattice parameter, b the Burgers vector and Z_{li} and a_{li} are parameters used to describe the evolution of the bias Z_{ic} with the size of the clusters.

The rate of emission of point defects from loops depends strongly on the binding energy $E_b(n)$. Results from molecular dynamics [8,9] can be accurately described by the following expression:

$$E_{bi}(n) = E_{fi} + \frac{E_{b2i} - E_{fi}}{2^{0.8} - 1}(n^{0.8} - (n-1)^{0.8}), \tag{6}$$

where E_{fi} is the formation energy of interstitial point defect, n the number of point defect in a cluster of size n and E_{b2i} is the binding energy for a cluster of size two.

Similar expressions can be obtained for vacancies.

As voids were experimentally detected (in a small amount) only in materials irradiated at 375 °C, their effect as sinks was not taken into account in the model.

The experimental observation that the initial dislocation network vanished during irradiation is consistent with an hypothesis of irradiation induced climb of dislocations allowing for their mutual annihilation. As a consequence, the density of dislocations is going to evolve according to the amount of point defects absorbed by the dislocations. To have a climb distance b for a density of dislocations ρ, the net number of point defects absorbed is ρ/b and the time required to obtain such a quantity of defects is $(\rho/b)/(\delta J)$. δJ is the excess of one type of point defects arriving on a density ρ of dislocations per unit time. The net climb velocity V can then be written as:

$$V = b/[\rho/b(\delta J)] = (\delta J)b^2/\rho. \tag{7}$$

The rate of annihilation of dislocations is proportional to the dislocation density ρ and inversely proportional to the time necessary to climb a distance $\rho^{-1/2}$.

A reasonable assumption is that δJ is proportional to ρ. The resulting evolution for the dislocation density is:

$$d\rho/dt = -Kb^2\rho^{3/2}. \tag{8}$$

This expression predicts that the density of dislocations will decrease as $1/t^2$. An estimation of K can be obtained from the dose necessary to evaporate the initial dislocation network.

Table 5
Irradiation parameters

Parameter	Values		
	OSIRIS	BOR-60	EBR-II
G (dpa/s)	2.9×10^{-7}	9.4×10^{-7}	1.4×10^{-6}
T (°C)	330	375	330
η	0.3	0.15	0.15
f_{i2}	0.5	0.5	0.5
f_{i3}	0.2	0.2	0.2
f_{i4}	0.06	0.06	0.06
f_{v2}	0.06	0.06	0.15
f_{v3}	0.03	0.03	0.7
f_{v4}	0.02	0.02	0.15

4.2. Parameter identification and predictions

The model described above involves a number of parameters. The parameters characterizing irradiation cascades are summarized in Table 5: they are specific for each reactors and, except for irradiation temperature, have only a limited influence [23].

The parameters which strongly influence the results are related to the materials: they control in particular the response to temperature, via the activation energies for diffusion, and the binding energies between point defects and clusters. These parameters are listed in Table 6. They have been identified in order to describe with a

Table 6
Material parameters

Parameters	SA304	CW316	CW316Ti	Intervals for experimental data	References
E_{mi}	**0.45 eV**	**0.43 eV**	**0.43 eV**	0.4–0.85	[10–14]
E_{mv}	1.35 eV	1.35 eV	1.35 eV	1.1–1.4	[10–16]
D_{0i}	10^{-3} cm^2/s	10^{-3} cm^2/s	10^{-3} cm^2/s	10^{-4}–10^{-2}	[10,11,17,18]
D_{0v}	0.6 cm^2/s	0.6 cm^2/s	0.6 cm^2/s	10^{-2}–1	[10,11,16,17,19]
E_{fi}	4.1 eV	4.1 eV	4.1 eV	4–5	[15]
E_{fv}	1.7 eV	1.7 eV	1.7 eV	1.2–2	[10–12,14–16]
E_{b2i}	**0.6 eV**	**0.6 eV**	**0.6 eV**	0–2	[10–12,20]
E_{b2v}	0.5 eV	0.5 eV	0.5 eV	0–2	[12,15,20]
r_{iv}	0.7 nm	0.7 nm	0.7 nm	0.4–0.65	[21]
Z_{li}	63	63	63	63	[11]
a_{li}	0.8	0.8	0.8	0.8	[22]
Z_i	1.1	1.1	1.1	1–1.1	[10,15,16]
Z_{lv}	33	33	33	33	[11]
a_{lv}	0.65	0.65	0.65	0.65	[22]
Z_v	1	1	1	1–1.1	[15]
ρ_0	**10^{10} m^{-2}**	**10^{14} m^{-2}**	**10^{14} m^{-2}**	10^{10}–10^{14}	
d	4×10^{-3} cm	4×10^{-3} cm	4×10^{-3} cm	10^{-3}–10^{-2}	

The values used for the model are compared with the range of experimental data available in the literature. The most sensitive parameters are indicated in bold type.

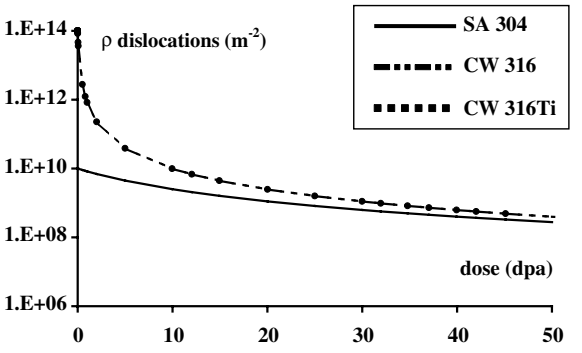

Fig. 5. Evolution of dislocation density for alloys in BOR-60.

reasonable accuracy the experimentally observed evolution of average size and density of interstitial loops.

All the parameters used in the model have a transparent physical interpretation and the values of the parameters are within the ranges of values reported in the literature, when available. After a parametric study, the most important parameters have been identified. These parameters are the irradiation temperature and the migration and binding energies of the point defects.

The value of the recovery constant K in Eq. (8) is obtained from the evolution of dislocation density as shown in Fig. 5. The values of K required to describe the evolution of dislocation density appear to depend mainly on the irradiation conditions for the standards SA304L and CW316 alloys. For the Osiris reactor, the BOR-60 reactor and the EBR II reactor, values are respectively 300, 970 and 14 400 m^{-1}. As expected an increase in flux or an increase in temperature induces a larger value of δJ and therefore a larger value of K. The case of the 316 alloy modified with titanium is interesting since the recovery rate at high temperature is substantially lower ($K = 1440$ instead of 14 400 m^{-1}). This indicates a possible role of titanium segregation limiting dislocation mobility.

The experimental curves for the density and the size of Frank loops are shown together with the model prediction for the three alloys and the two temperatures in Figs. 6 and 7. The predicted density of vacancy loops is at least three orders of magnitude lower than the density of interstitial loops, in agreement with the experimental observation: indeed, only interstitial Frank loops are observed. The size of the vacancy loops however is much too large: it is likely that the transformation of vacancy clusters into voids takes over from the growth of vacancy loops.

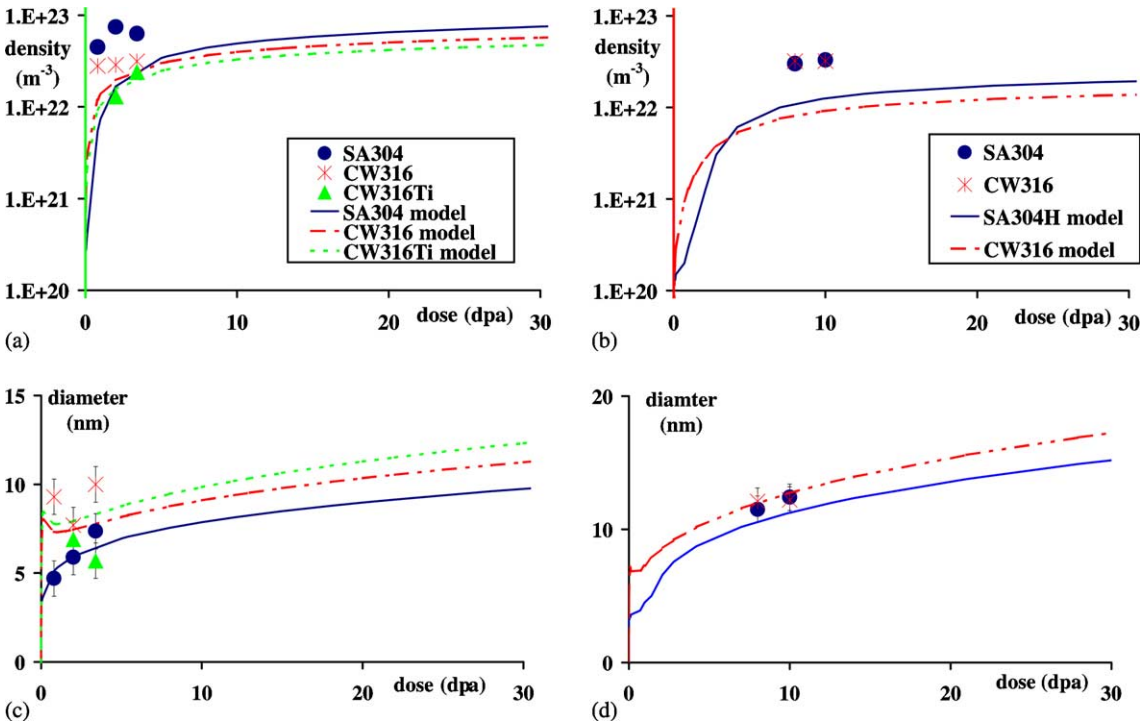

Fig. 6. Evolution of Frank loops density ((a) and (b)) and diameter ((c) and (d)) for low doses.

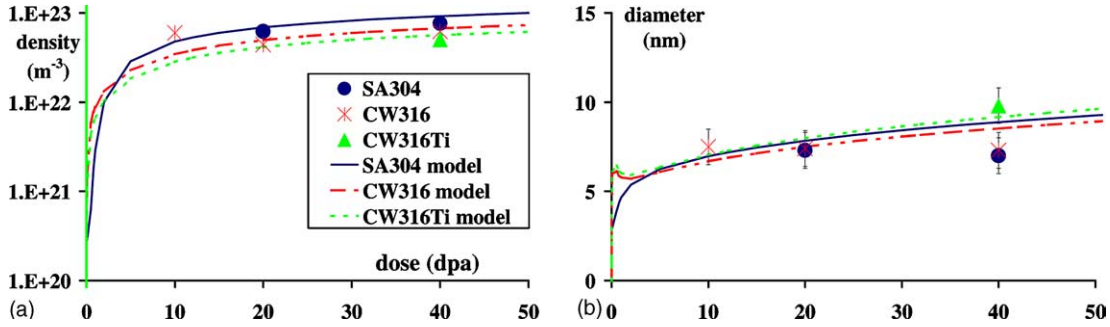

Fig. 7. Evolution of Frank loops density (a) and size (b) for high doses.

The model parameters were identified by adjusting the model to the experimental observations at low doses, as shown in Fig. 6. The same parameters were then used to predict the evolution for higher doses shown in Fig. 7. It must be noted that the parameters used to fit the low doses at 330 °C in OSIRIS reactor are the same that allow the prediction of the microstructure for low and high doses for the BOR-60 reactor at the same temperature, although this reactor has different flux and spectrum. It is apparent also that recovery plays an important role in the microstructural evolution. A failure to account for the recovery of the initial dislocation network would lead to a faster saturation of the loop structure in the 316 alloys, and the model would not be able to describe accurately both the low and high doses with the same parameters.

The most sensitive parameters controlling the irradiation microstructure are the temperature, the doses, the materials constants and the initial microstructural state in terms of the dislocation density.

5. Conclusions

A systematic experimental quantitative characterization of irradiation induced microstructures in austenitic stainless steels has been performed for different irradiation conditions in terms of temperature, fluxes, doses and energy spectra. These results have been analyzed using a cluster dynamics model specially adapted to account for the evolution of dislocation substructure, and to deal with large doses.

All the parameters in the model have a transparent physical interpretation. The values of the parameters are identified to fit correctly the low doses results and are within the ranges of values reported in the literature, when available. The prediction of the microstructures at high doses are in good agreement with the measured values, and the most sensitive parameters have been identified: irradiation temperature, dose, and the migration and binding energies of the point defects. The initial microstructure in terms of dislocation densities, has also been identified as an important feature.

The present model is well suited for the interstitial loops but fails to describe accurately the vacancy clusters, and notably their transformation into voids: further work is required in this respect, accounting for the possible role of gases.

By nature, such models are restricted since they describe localized sinks as grain boundaries and dislocation network, in a continuum manner. Features such as the spatial distribution of irradiation defects (loop free zones close to the boundaries for instance) which may be relevant to the question of grain boundary failure, cannot be accounted for. The exact expression of the sink efficiency modified by a finite density of defects is also likely to be very primitive. Coupling these approaches with Monte Carlo simulation on events could improve substantially the description.

In paper II, we will now investigate the consequences or the irradiation induced microstructure on the yield stress.

Acknowledgements

Enlightening discussions with Dr G. Martin, Dr P. Bellon, Dr R. Cauvin and Dr Ch. Domain are gratefully acknowledged. Authors are also grateful to Dr G.R. Imel at ANL, US, for performing neutron irradiation in EBR-II reactor and to Dr V. Golovanov and Pr V. Shamardin at RIAR, Russia, for performing neutron irradiations in BOR-60 reactor. This work was performed in the frame of the French R&D Project 'PWR Internals' sponsored by Electric Power Research Institute (MRP/Joint Owner Baffle Bolts Program), Palo Alto, CA, under the responsibility of Dr H. T. Tang, whose support is gratefully acknowledged.

Appendix A

Table of notations

Parameter	Signification
G	Flux
T	Temperature
η	Recombination in the cascades
f_{i2}	Bi-interstitials in the cascades
f_{i3}	Tri-interstitials in the cascades
f_{i4}	Quadri-interstitials in the cascades
f_{v2}	Bi-vacancies in the cascades
f_{v3}	Tri-vacancies in the cascades
f_{v4}	Quadri-vacancies in the cascades
E_{mi}	Migration energy for interstitials
E_{mv}	Migration energy for vacancies
D_{0i}	Pre-exponential coefficient for the diffusion of interstitials
D_{0v}	Pre-exponential coefficient for the diffusion of vacancies
E_{fi}	Formation energy for interstitials
E_{fv}	Formation energy for vacancies
E_{b2i}	Binding energy for the bi-interstitials
E_{b2v}	Binding energy for the bi-vacancies
r_{iv}	Recombination radius between defects
Z_{li}	Bias factor of the loops for interstitial
a_{li}	Parameter for Z_i
Z_i	Bias factor of dislocations for interstitial
Z_{lv}	Bias factor of the loops for vacancies
a_{lv}	Parameter for Z_v
Z_v	Bias factor of dislocations for vacancies
ρ_0	Initial dislocation density
d	Grain size
b	Burgers vector
a	Lattice parameter
d	Grain size

References

[1] P. Scott, J. Nucl. Mater. 211 (1994) 101.

[2] Les Aciers Inoxydables. Les éditions de Physique 1990, ISBN: 2-86883-142-7, Editeurs scientifiques Lacombe, Baroux, Béranger, p. 132.

[3] D.J. Edwards, E.P. Simonen, S.M. Bruemmer, 9th International Conference on Environmental Degradation of Nuclear Materials in Nuclear Power Systems-Water reactors, Newport Beach, California, 1–5 August 1999.

[4] W.J. Phythian, R.E. Stoller, A.J.E. Foreman, A.F. Calder, D.J. Bacon, J. Nucl. Mater. 223 (1995) 245.

[5] D.J. Bacon, F. Gao, A.V. Barashev, Y.N. Osetsky, Mater. Res. Soc. Symp. Proc. 540 (1999) 617.

[6] A.D. Brailsford, R. Bullough, AERE Harweport TP 854 (1980).

[7] A. Hardouin Duparc, C. Moingeon, N. Smetniansky-de-Grande, A. Barbu, J. Nucl. Mater. 302 (2–3) (2002) 143.

[8] N. Soneda, T. Diaz de la Rubia, Philos. Mag. A 78 (5) (1998) 995.

[9] Y.N. Osetsky, A. Serra, M. Victoria, S.I. Golubov, V. Priego, Philos. Mag. A 79 (9) (1999) 2285.

[10] T. Katoh, A. Kohyama, R.E. Stoller, C. Namba, J. Nucl. Mater. 222–237 (1996) 1022.

[11] R.E. Stoller, G.R. Odette, in: F.A. Garner, N.H. Packan, A.S. Kumar (Eds.), Radiation induced changes in microstructure: 13th international symposium (Part I), ASTM STP 955, American Society for Testing and Materials, Philadelphia, 1987, p. 371.

[12] W. Schüle, R. Scholz, in: International Conference on Mechanical Behaviour and Nuclear Applications of Stainless Steel at Elevated Temperatures, 20–22 May 1982, Metals Society, Varese (Italy), 1982, p. 141.

[13] N. Yoshida, J. Nucl. Mater. 205 (1993) 344.

[14] C. Dimitrov, O. Dimitrov, J. Phys. F: Met. Phys. 14 (1984) 793.

[15] N.M. Ghoniem, D.D. Cho, Phys. Stat. Sol. (a) 54 (1979) 171.

[16] K. Krishan, N.N. Thieu, Radiat. Eff. 100 (1986) 249.

[17] M.J. Caturla, N. Soneda, E. Alonzo, B.D. Wirth, T. Diaz de la Rubia, J.M. Pelardo, J. Nucl. Mater. 276 (2000) 13.

[18] J. Gan, G.S. Was, R.E. Stoller, J. Nucl. Mater. 299 (2001) 53.

[19] H. Trinkaus, B.N. Singh, A.J.E. Foreman, J. Nucl. Mater. 206 (1993) 200.

[20] E.A. Koptelov, S. Ishino, S. Iwata, N. Sekimura, J. Nucl. Mater. 225 (1995) 38.

[21] A. Hardouin-Duparc, Etude de la formation sous irradiation des amas de défauts ponctuels dans les aciers ferritiques faiblement alliés, PhD thesis, rapport CEA-R-5791.

[22] Coghlan, Yoo, Radius dependence of the sink strength of a dislocation loop, symposium on the role of dislocation modelling physical system, Florida, 1980.

[23] C. Pokor, Caractérisation microstructurale et modélisation du durcissement des aciers austénitiques irradiés des structures internes des réacteurs à eau pressurisée. PhD Thesis, Institut National Polytechnique de Grenoble, France, 2002.